SUPPLEMENTAL INFORMATION

Supplemental Data

Figure S1. PrP^C is Transported Along Axons. Related to Figure 1.

(A) Schematic diagram of a sciatic nerve ligation experiment. After ligation, proteins moving in an anterograde direction accumulate in the proximal side of the ligature, while those traveling in the retrograde direction accumulate in the distal side.

(B) Confocal images of longitudinally sectioned ligated and unligated mouse sciatic nerves fixed and stained with antibodies against PrP^C and APP. PrP^C and APP accumulated primarily at the proximal end of the ligature. Arrows point to ligation site.

(C) Schematic diagram of the MoPrP.Xho::YFP-PrP (referred to as YFP-PrP^C) construct made to image YFP-PrP^C vesicle transport in hippocampal mouse cells. Top panel shows a diagram of PrP^C protein structure indicating the signal peptide (SP) sequence, coding sequence (PrP^C), and GPI anchor sequence. Both SP and GPI sequences are cleaved post-translationally. The letters between the SP and YFP are linker amino acids. The numbers below indicate position of amino acid residues (2-227 for YFP; 23-231 for PrP^C coding sequence).

(D) Confocal image of a mouse N2a cell transfected with YFP-PrP^C and fixed and stained with an antibody against PrP^C and an Alexa-568 secondary antibody. Cell was permeabilized prior to staining. Arrowheads indicate vesicles in both channels that colocalize. Some vesicles reside in a different optical slice in either one or the other channel.

(E) Extracts of N2a cells transfected and non-transfected with the YFP-PrP^C construct. For each condition, cells were either treated or not with PNGase F to deglycosylate PrP^C and YFP-PrP^C.

Figure S2. Reduction of DHC1 by shRNA does not Change Segmental Velocities. Related to Figure 2.

(A) N2a cells were transfected with a lentiviral construct containing a shRNA against DHC1 or a scrambled control. Cells were harvested 2 days post-transfection and RNA was extracted to perform qRT-PCR. Percentage of DHC1 mRNA for both conditions using two different primer sets, is shown.

(B) Deconvolved images of hippocampal cells transfected with a DHC1 shRNA-mCherry construct to reduce DHC1 levels and stained with antibodies against DHC1 and PrP^C. (a) Red arrow points to mCherry signal in transfected cell; (b) Green arrow points to untransfected cell stained with an antibody against DHC1 showing higher levels than the shRNA DHC1-mCherry transfected cell in (a); (c) Same cells stained with an antibody against PrP^C to show cell shape; (d) Merge of mCherry and DHC1 antibody signals from (a) and (b). In cells expressing DHC1 shRNA-mCherry, DHC1 protein levels were reduced by 50-80%, for an average of 66%, as compared to non-mCherry cells.

(C) Anterograde and retrograde mean segmental velocities of PrP^C vesicles moving in axons are not affected after treatment with the DHC1 shRNA-mCherry construct validated in (A).

Figure S3. Differential Requirements of Kinesin-1 Subunits in the Intracellular Transport of YFP-PrP^C and Synaptophysin-mCherry or Synaptophysin-YFP Vesicles. Related to Figure 3.

(A-C) Anterograde and retrograde mean segmental velocities for (A) all moving YFP-PrP^C vesicles (bi- and uni-directional), (B) YFP-PrP^C vesicles moving uni-directionally (anterograde or retrograde), and (C) only YFP-PrP^C vesicles reversing at least once during the duration of our recording.

(D-F) Anterograde and retrograde mean segmental velocities of synaptophysin[a] vesicles in (D) KLC mutants, (E) Kinesin-1A and Kinesin-1C mutants, and (F) Kinesin-1B mutants. All moving (unidirectional and reversals) vesicles are included.

(G-I) Average percent synaptophysin[a] cargo population for anterograde, retrograde, reversing and stationary cargo.

Nv = # vesicles; Numbers of segments are indicated inside bars.

All values are shown as mean ± SEM. ***p<0.001, **p<0.01, *p<0.05, permutation t-test (black asterisks), Wilcoxon-Mann-Whitney test (red asterisks).

[a] Data correspond to the movement dynamics of synaptophysin-mCherry for all conditions except for KLC2 shRNA-mCherry, in which case the behavior of synaptophysin-YFP was recorded.

Figure S4. Generation of a Kinesin-1C Deletion Null Mutant Mouse, and Kinesin-1B mutant Cells. Related to Figure 4.

(A) Schematic diagram of Kinesin-1C gene targeting vector, which was constructed as a deletion mutant. In the targeted allele, two Kinesin-1C exons encoding amino acid 132 to the first two nucleotides of amino acid 196 were replaced with a pGK-neo cassette. PCR genotyping primers are indicated by the red arrows.

(B) Kinesin-1C mRNA (Northern blot, left panel), and protein (Western blot, right panel) were absent from homozygous mutant Kinesin-1C mice brain lysates. Kinesin-1A and 1B protein levels were unchanged in the Kinesin-1C null mutant.

(C) DNA gel showing genotyping bands for Kinesin-1B hippocampal cell extracts treated with 0, 100, or 400 multiplicity of infection (MOI) units of cre-recombinase adenovirus. The Kinesin-1B II/II product is excised upon cre-treatement to convert to a Kinesin-1B I/I product. The larger PCR product of the Kinesin-1B I/I band is detected because of the position of the primers. Bottom arrow shows wild-type Kinesin-1B.

(D) Western blot showing reduction in the expression of Kinesin-1B protein in 100, and 400 MOI cre-treated hippocampal cells.

Figure S5. Intensity Distributions of Motor Subunits on PrP^C Vesicles Reveal a Heterogeneous Composition. Related to Figure 5.

(A) Scatter plot showing a linear relationship between normalized KLC1 Gaussian intensity amplitudes and KLC1 copy number. Gaussian amplitudes were obtained from the 'motor colocalization' program following KLC1 immunofluorescent staining of individual vesicles in hippocampal axons. KLC1-/- axons have 0 KLC1 copy number (N_{axons} = 10; Nvesicles = 237), KLC1 +/- axons have 1 KLC1 copy number (N_{axons} = 10; Nvesicles = 326), and KLC1+/+ axons have 2 KLC1 copy numbers (N_{axons} = 10; Nvesicles = 391).

(B) Western blot showing specificity of KLC1 antibody for increasing loaded amounts of KLC1 protein from mouse brain homogenates. KLC1 antibody recognizes a single band in wildtype (KLC1 +/+), but no band is recognized in KLC1 -/- homogenates.

(C) Scatter plot showing a linear relationship between KLC1 intensities and increasing loaded amounts of KLC1+/+ mouse brain homogenate. Intensities were measured from the Western blot in (B).

(D) Western blot showing DHC1 and tubulin (control) staining of N2a cell homogenates from cells transfected with DHC1 shRNA-mCherry or scrambled control constructs.

(E) Scatter plot showing linear relationships between DHC1 intensities (divided by tubulin intensities for the same loadings), and increasing loaded amounts of N2a cell homogenate from cells transfected with scrambled or DHC1 shRNA-mCherry constructs (to reduce DHC1 levels). Intensities were measured from the Western blot in (D).

(F, G) Intensity distributions of the percentage of PrP^C vesicles with (A) KLC1, when only KLC1 or both KLC1 and DHC1 are present; and with (B) DHC1, when only DHC1 or

both motor KLC1 and DHC1 are present. Nv = # vesicles.

(H) Distribution of PrP^C vesicles in Kinesin-1C -/- cells with one or both KLC1 and DHC1. Numbers in boxes are percentages of PrP^C vesicles that fall within each category. Color gradient represents higher to lower percentage of PrP^C vesicles in each category.

Movie S1. Bidirectional Movement of PrP^C Vesicles in a Wild-type Hippocampal Axon. Related to Figure 1. A streamline acquisition video of YFP-PrP^C vesicle transport in a 10 day-old hippocampal wild-type axon. Cell body is toward the left, terminus is toward the right. Movie was taken at 0.1 sec/frame, for 15 seconds.

Movie S2. Live Fixation of PrP^C Vesicles in a Microfluidic Chamber Microchannel. Related to Figure 6. A streamline acquisition video of YFP-PrP^C vesicle transport in a 10 day-old hippocampal wild-type axon growing through a microchannel of a microfluidic chamber. Cell body is toward the left, terminus is toward the right. Paraformaldehyde was applied to media approximately 20 seconds after beginning of movie acquisition. Paraformaldehyde fixes vesicular movement, temporarily quenching YFP signal.

Table S1. Segmental Velocity Modes Predicted for PrP^C Vesicle Transport in Kinesin-1 and Dynein Mutant Axons. Highlighted in gray is the proportion of segments in each condition that shift from higher to lower velocity modes.

SUPPLEMENTAL EXPERIMENTAL PROCEDURES

Sciatic Nerve Ligations

We confirmed earlier observations that the mammalian prion protein is transported in the sciatic nerve by using a protein accumulation paradigm in which nerves were ligated at the midsection, and proximal and distal sections were dissected

and analyzed for PrP^C immunofluorescence 6 hours post-ligation (Figure S1A). In this assay, proteins that travel in anterograde and retrograde directions accumulate at the proximal and distal side of the ligations, respectively. For each wild-type mouse, one sciatic nerve was ligated approximately at the midsection while the other was left un-ligated. Six hours post ligation, mice were sacrificed and either 3 mm of nerve at either side of the ligation, or 6 mm of un-ligated nerve were removed. Nerves were embedded with Histo Prep (Fisher) and immersed immediately in methanol/dry ice and maintained at -20˚C. Nerves were cut longitudinally in a cryostat at -20˚C, fixed with 4% paraformaldehyde and stained for antibodies against PrP^C and APP. We found that PrP^C accumulated primarily in the proximal side of nerves suggesting that net movement in the nerve is toward the terminal (Figure S1B).

Molecular Cloning

As the signal peptide (SP) and GPI anchor sequences are cleaved off from the 5' and 3' ends of PrP^C during normal processing, YFP and linker sequences were inserted between the signal peptide and the rest of the mouse PrP^C sequence to avoid cleavage of YFP (Figure S1C). YFP was annealed by PCR amplification to the 5' end of amino acid 23 of the PrP^C sequence with a XhoI site at the 3' end (YFP-PrP^C-XhoI). The signal peptide (amino acids 1-22, nucleotides 1-66) was amplified by PCR together with the adjacent 10 nucleotides 5' of the coding region (ATCAGTCATC), and with the addition of XhoI sites 5' of the amplicon (XhoI-SP). These two PCR fragments (YFP-PrP^C-XhoI and XhoI-SP) were annealed together by overlapping PCR amplification which resulted in the addition of a linker between the two amplicons. The resulting sequence (XhoI-SP-linker-YFP-PrP-XhoI) was cloned into the XhoI site of vector MoPrP.Xho which contains the promoter, 5' intronic, and 3' untranslated sequences of the murine prion protein gene (Borchelt et al., 1996).

To determine whether our construct behaved similarly to endogenous PrP^C, we transfected differentiated mouse neuroblastoma (N2a) cells with YFP-PrP^C, and fixed and stained them with antibody Hum-D13 against PrP^C. We found that ~90% of endogenous PrP^C vesicles colocalized with YFP-PrP^C (Figure S1D). We further tested YFP-PrP^C for the common post-translational addition of glycosylation groups that endogenous PrP^C undergoes in the Golgi. We found that treatment of N2a cells with the peptide N-glycosidase PNGase F removed the glycosylated isoforms both in endogenous (non-transfected) and N2a cells transfected with YFP-PrP^C, showing that YFP-PrP^C is post-translationally glycosylated (Figure S1E). Finally, the levels of YFP-PrP^C in transiently transfected N2a cells was ~88% that of endogenous PrP^C, thus indicating that transient transfection does not result in highly over-expressed levels of this transgene (Figure S1E). The high degree of co-localization, deglycosylation profiles, and overall expression levels indicate that YFP-PrP^C behaves and is being processed similarly to the endogenous protein.

Mice

Generation of Kinesin-1C Null Mice.

Homozygous Kinesin-1C null mice were generated in our lab by replacement targeting. Adult Kinesin-1C -/- mice do not exhibit any gross morphological abnormalities and live through adulthood as homozygous null mutants.

Constructing the Kinesin-1C Targeting Vector. A Kinesin-1C genomic clone (KIF5g-G) isolated from a mouse 129SVJ/Lambda FIX II genomic library (Stratagene) was used to construct a simple replacement targeting vector. The targeting vector was made as follows: the right arm was a 3.6 kb SmaI-ScaI-ScaI fragment. This fragment was made by subcloning SmaI-ScaI and ScaI-ScaI fragments into pBluescript SK vector, then being ligated together, the right arm was subcloned into the BamHI site of pPNT vector by blunt ligation. A 4.5 kb SmaI-SmaI fragment was blunt ligated into XhoI site of right-

arm/pPNT, and this fragment containing two exons (encoding amino acid #132 to the first two nucleotides of aa #196) with a ~2 kb pGK-neo cassette, and was named as KIF5C-KO/pPNT.

Generating Chimeric Mice. The Kinesin-1C targeted ES cells were generated as described by Klein et al. (Klein et al., 1993). The KIF5C-KO/pPNT plasmid DNA was linearized with NotI, and transfected into RI ES cells by electroporation, 200 ug/ml G418 was added ~36 hours after transfection, and 2 uM gancyclovir was added one day later for the negative selection. Surviving clones were screened by Southern blot analysis of HindIII-digested ES DNAs with a 3'-external probe. Two positive clones were isolated by two independent transfections: K128 (one out of 240 clones screened), and #157 (one out of 180 clones). Clone K128 was injected into C57BL/6J blastocysts to produce chimeras, and germline transmitted heterozygous Kinesin-1C mice were generated by crossing male chimeras to C57Bl/6J mice.

Kinesin-1B Mice

Kinesin-1B null/Pflox mice (type I deletion; hereafter referred as Kinesin-1B I/+), and conditional homozygous Kinesin-1B pflox mice (type II deletion; hereafter referred as Kinesin-1B II/II), were generated by Nancy Jenkings and JianDong Huang (Cui et al., 2010). These mice were maintained as heterozygous (Kinesin-1B I/+), or as conditional homozygotes (Kinesin-1B II/II). Kinesin-1B I/+ intercrosses produced no Kinesin-1B I/I mice (n = 87; Nancy Jenkins, unpublished data), likely due to early embryonic lethality which is in agreement with earlier reports of Kinesin-1B homozygote lethality at E9.5 (Tanaka et al., 1998). Genotyping of cre-treated cells showed a shift from the II/II to the I/I null mutant genotype 3 days after adenovirus treatment (Figure S4C). This shift was confirmed by qPCR, which showed 80% and 88% reduction of II/II genotype after treatment with 100 and 400 MOI, respectively. Immunobloting of treated cell lysates also showed reduction in protein levels by ~ 50% (Figure S4D).

Cell Culture

Hippocampal cells were dissected from one-day old neonates for all mice except from KLC1 -/- and Kinesin-1A -/- mice. Because most KLC1-/- and all Kinesin-1A-/- neonate pups die immediately upon birth, hippocampal neurons were dissected from E18-E21 embryos (Rahman et al., 1999; Xia et al., 1998). Hippocampi were dissected, treated with Papain (Worthington), dissociated by trituration, and plated on poly-L-lysine treated glass coverslips, as described previously (Falzone et al., 2009). Cells were plated on DMEM medium containing 10% fetal bovine serum (FBS) for 1-3 hours, and switched to Neurobasal-A media containing B27 complement and Glutamax (Invitrogen). Neurons were cultured for 10 days at 37˚C and in a 5.5% CO_2 atmosphere prior to transfection and imaging. For live tracking imaging studies, cells were plated in 24-well glass coverslips at a density of ~125,000 cells per well.

Antibodies

The antibody against PrP^C (Hum-D13) was obtained from InPro and also as a gift from A. Williamson and Laura Solforosi (The Scripps Research Institute; (Peretz et al., 1997). Antibodies against KLC1 (V-17) and DHC1 (sc-9115) were from Santa Cruz Biotechnology. Anti-Kinesin-1A, and anti-Kinesin-1C antibodies were described previously (Rahman et al., 1998; Xia et al., 2003). Kinesin-1B antibody is a rabbit polyclonal raised against amino acids 499-783.

Primary antibodies used for motor colocalization immunofluorescence experiments PrP^C (Hum-D13), KLC1 (V-17), DHC1 (sc-9115), were used at a 1:100 dilution. The corresponding secondary chicken anti-human (FITC), donkey anti-goat (Alexa 647), and donkey anti-rabbit (Alexa 568) antibodies were used at a dilution of 1:200, respectively. These antibody dilutions were chosen after obtaining antibody saturation curves using different primary and secondary antibodies dilutions to determine the optimal combinations. Primary and secondary antibody-only controls were done for

all possible antibody combinations to test for antibody cross-reactivity. We observed only background levels in axons with primary and secondary antibody-only staining.

For the motor colocalization studies, to assess KLC1 antibody specificity and whether there was a linear correlation between KLC1 intensities and KLC1 copy number by immunofluorescence, KLC1+/+, KLC1+/-, and KLC1-/- hippocampal cells were stained with antibody KLC1 (V-17). KLC1 levels were quantified on all KLC1-associated vesicles after estimation of Gaussian curves for each point source. Mean KLC1 intensity in KLC1 -/- vesicles was reduced by >60% as compared to KLC1 +/+ vesicles, after background subtraction (93.82 arbitrary units [au] in KLC1 +/+; 65.42 au in KLC1 +/-, and 36.94 au in KLC1 -/- axons). Furthermore, the KLC1 intensity signal increased with increasing KLC1 copy number, and this relationship was linear with a high regression coefficient ($R^2 = 0.99$), suggesting that relative quantitation of KLC1 levels is possible to assess with this antibody (Figure S5A). Furthermore, while it is possible that the residual KLC1 signal observed in KLC1-/- axons might be attributed to unspecific binding of the antibody, Western blot assays from KLC1 -/- mouse brain homogenates show high antibody specificity (Figure S5B), suggesting that the remaining signal corresponds to background fluorescent levels. We also observed a linear relationship between amounts of KLC1 detected with the same KLC1 antibody (V-17) and KLC1 copy number in Western blots of mouse brain homogenates (Figure S5C). In addition, we co-stained hippocampal neurons with antibodies against KLC1 and mitochondrial Cox1, and found no significant colocalization between the two markers, in agreement with reports that mitochondrial transport is independent of KLC1 function (Glater et al., 2006), and further suggesting that the KLC1 antibody was specific.

For motor colocalization studies, to assess DHC1 (sc-9115) specificity, we stained hippocampal cells transfected with a scrambled control or a DHC1 shRNA-mCherry construct to reduce the function of DHC1 (see shRNA section below).

Quantitation of immunofluorescent staining of DHC1 levels of transfected versus non-transfected cell bodies 2 days post transfection indicated that DHC1 signal was reduced from 50-80%, for an average of 66% (n = 13; Figure S2B). Furthermore, DHC1 mRNA levels were reduced by >80% from N2a cells transfected with the same DHC1 shRNA-mCherry construct (Figure S2A, see shRNA section below). To test that our DHC1 antibody was in a linear range, increasing amounts of DHC1 shRNA-treated and scrambled-treated N2a cell homogenates were loaded and analyzed by Western blot using a DHC1 antibody (Figure S5D). Quantitation of DHC1 levels normalized to alpha-tubulin (DM1α) showed a linear relationship between DHC1 intensities and increasing amounts of loaded N2a cell homogenate, suggesting that this antibody behaves in a linear range and that relative quantitation of DHC1 levels is possible to assess with this antibody (Figure S5E).

Vesicle Immunoisolations

Wild-type mouse brains were homogenized in a detergent-free buffer (8% sucrose and 3mM imidazole, pH 7.4), and post-nuclear supernatant (PNS) was bottom-loaded on a sucrose step gradient consisting of 35%, and 8% sucrose. After centrifugation at 200,000 g for 2 hours at 4˚C, the 8/35 interphase was harvested and incubated overnight with antibodies against KLC1 (V-17, Santa Cruz Biotechnology), or GFP (A6455, Molecular Probes). Protein A or G agarose beads (Roche) were added and fractions were incubated for 2 hours at 4˚C. Washed pellets were eluted with beta-mercaptoethanol (BME) and boiled, and eluted samples were analyzed by SDS-PAGE and Western blot.

shRNA

Three shRNA constructs for each KLC2, DHC1, and scrambled D11 targets were built as part of a kinesin and dynein lentiviral mini-library, in a pLL3.7 GW lentiviral vector with gateway entry modifications and a mCherry marker (S.E.E., unpublished data).

Target sequences were designed by Tony Orth at the Genomics Novartis Foundation using proprietary software that identified and selected sequences after comparison of each to the entire mouse genome to ascertain a high degree of specificity (or no-specificity in the case of the scrambled sequence). Validation of shRNA constructs for reduction of KLC2, and DHC1 function was done by transfecting N2a cells separately with the 3 sequences of each target using Lipofectamine 2000 (Invitrogen). Transfection rates varied from 50-70%, and were ascertained by counts of mCherry fluorescence on cell bodies. Cells were harvested 2-4 days post-transfection and lysates were immunoblotted with antibodies against KLC2 (63-90), and DHC1 (sc-9115, Santa Cruz Biotechnology). N2a cells were also harvested at the same time points and RNA made by reverse-transcriptase (RT) PCR using a SuperScript First Strand kit (Invitrogen). Quantitative PCR was performed to test for reduced mRNA of KLC2 and DHC1 using 3 sets of primers designed for each. One sequence was selected for each target and co-transfected with either YFP-PrP^C or synaptophysin-YFP using Lipofectamine 2000, in 10-day old hippocampal neurons 18-24 hours prior to imaging. Only cells with mCherry fluorescence were imaged for YFP-PrP^C or synaptophysin-YFP vesicle transport. To further validate decreased levels of DHC1 protein in hippocampal cells transfected with the chosen DHC1 shRNA-mCherry construct, we fixed and stained transfected cells with an antibody against DHC1. Quantitation of immunofluorescent staining of DHC1 levels of transfected versus non-transfected cells was done as detailed above.

The sequences used in shRNA constructs were the following: KLC2 (forward 5'-GTGGAATACTACTACCGGA-3'; reverse 5'- AGGTGGAATACTACTACCGGAGA-3'); DHC1 (forward 5'- GTGATGCCATACGAGAGAA-3'; reverse 5'-CAGTGATGCCATACGAGAGAAGA-3'); scrambled D11 (forward 5'-GCACACGTATCGACGTATC-3'; reverse 5'-CGCACACGTATCGACGTAT-3'). We observed nearly ~95% co-transfection (n = 25 cells) between YFP-PrP^C and KLC2 or

DHC1 shRNA-mCherry, and 50-70% transfection efficiency in N2a cells, which produced an estimated ~83% and ~89% reduction of KLC2 and DHC1 mRNA expression, respectively, 2 days after transfection, as confirmed by RT-QPCR (Figure S2A and data not shown). Protein levels were reduced by >90% and >66% for KLC2 and DHC1, respectively (Figure S5D, and data not shown).

Mouse N2a cells used for validation of KLC2, and DHC1 shRNAs were cultured in DMEM containing 10% FBS and 5% penicillin-streptomycin at 37˚C in 5% CO_2. Cells were plated at 40-50% confluency and transfected with shRNA target constructs 18-24 hours later with Lipofectamine 2000.

Live Imaging Microscopy, Motor Colocalization, and Vesicle Mapping

Live imaging of YFP-PrP^C, synaptophysin-mCherry, or synaptophysin-YFP was done on 10 or 11-day old hippocampal neuron axons, within 24 hours after transfection. Transfection rates were ~3%, which facilitated imaging of single axons. Plates were maintained at 37˚C and in a 5.5% CO_2 environment throughout the imaging period, for a maximum of 40 minutes. Images were taken exclusively from axons and we distinguished axons from dendrites by morphology. Axons are thinner and uniform in diameter, are longer, have fewer branches, and exhibit prominent growth cones (Baas et al., 1989; Baas et al., 1988). Axons were traced from termini to cell body and imaged within a region >180 um from either end. Live images were taken with a Nikon Eclipse TE2000-U inverted microscope equipped with a Coolsnap HQ camera (Roper Scientific) and a 100X/1.4 NA oil objective. Movies were 15 seconds long and collected at 10 frames per second at 100ms exposure (10Hz), at a resolution of 0.126um using Metamorph stream acquisition software (MDS Analytical Technologies).

For motor colocalization studies, cells were fixed with 4% paraformaldehyde plus 4% glucose, for 30 minutes at 37˚C and in a 5.5% CO_2. Cells were incubated for 5 minutes at room temperature with 0.1% triton X-100 (TX-100) for permeabilization, and

followed by a 45 minute incubation in block consisting of 10% donkey serum, 3% BSA, 0.1% TX-100 in PBS. Images of fixed wild-type and Kinesin-1C -/- hippocampal cells stained with antibodies against PrP^C, KLC1 and DHC1 were taken on the same day and under the exact exposure conditions for each experimental condition. Fixed immunofluorescence images were taken on a Deltavision RT deconvolution system mounted on an Olympus IX70 inverted microscope equipped with a mercury lamp, with bandpass excitation and emission filters for FITC, Rhodamine and Cy-5 and a 100X objective/1.4 NA PlanApo. Images of 0.5 mm TetraSpeck fluorescent microspheres (Invitrogen), which were used to calibrate the X-Y-Z alignment of the microscope to account for spherical and chromatic aberration of the fluorescent channels, were also collected on the same day. For some colocalization analyses, fluorescent intensity calibration between experiments was done using 2.5 μm green, red, and deep red 0.3% relative intensity fluorescent microspheres from an InSpeck Microscope Image Intensity Calibration Kit (Invitrogen).

For vesicle mapping analyses, hippocampal neurons (~275,000) were plated in microfluidic chambers as described previously (Taylor et al., 2005). Movies of intracellular YFP-PrP^C movement from transfected cells were taken as described above, from axonal regions inside microchannels. While live imaging, culture media was removed from chambers and replaced with 4% paraformaldehyde to fix neurons and stain with KLC1 and DHC1 antibodies. Images of YFP-PrP^C, KLC1 and DHC1 channels from fixed axons were taken from the exact location where live movies were acquired, and these images were subsequently mapped back onto kymographs of the live YFP-PrP^C movement using Adobe Photoshop. Individually mapped YFP-PrP^C vesicles were classified according to transport class (anterograde, retrograde or stationary), and were fitted with Gaussians. The X-Y coordinates of each mapped PrP^C vesicle were used to determine co-localization with KLC1 and/or DHC1 Gaussian-fitted point sources. The

combination of live and fixed analyses was used because simultaneous live visualization of motor and vesicle movement via co-expression of fluorescent tags attached to motors is challenging due to the overwhelming signal of presumably inactive soluble motors that results in a non-localized cytoplasmic fluorescence.

Data Analysis

Particle Tracking Definitions

For each genotype, trajectories were classified as anterograde, retrograde, stationary or reversing, and five parameters describing the dynamics of transport were calculated: percent cargo population, segmental velocity, run length, pause frequency, and pause duration. Switch frequency and estimated run length were also calculated for some genotypes. We used a custom MATLAB based particle tracking software (LAPTrack) to track the trajectories of vesicles (Reis et al., unpublished data). The following definitions were used for the calculation of transport parameters:

Track. A cargo trajectory represented by its X and Y coordinate series, that lasts through all frames of the imaging period (15 seconds, 150 frames).

Track Segment. An uninterrupted period of anterograde or retrograde movement with a speed of > 0.095 μm/sec framed by pauses and/or the beginning of an imaging period.

Pause. A cargo undergoes a pause when, at a particular position, has an instantaneous velocity of < 0.095 μm/sec, within a sliding window width of 7 frames.

Stationary Vesicle. A particle that is paused for the entire duration of the imaging period (15 seconds).

Reversal (Switch) Vesicle. We define a cargo as undergoing a reversal at coordinates X, Y, if the two vectors that meet at that location (a) point in opposite directions, and (b) are located a minimum of 550nm away from X, Y. This minimum threshold distance allows

us to avoid false positives in reversal detection caused by small local random movement.

Segmental velocity (in μm/second). The total distance of a track segment divided by the segment duration. Anterograde or retrograde segmental velocities include those from segments moving uniquely in either direction, as well as those segments from the anterograde or retrograde direction of reversal tracks.

Run Length (in μm). Is the distance moved by a particle in a defined segment. Run length is calculated for individual segments and then pooled together for each genotype. Standard error is calculated separately for anterograde and retrograde directions pooling data from all tracks.

Duration-weighted Segmental Velocity (in μm/second). Is a weighted average of segmental velocities by the duration of movement. Thus, they are calculated as the sum of the segmental velocities per track, multiplied by their durations, and divided by the sum of the durations for that particular track. This parameter is calculated for anterograde and retrograde segments (including reversals), and mean and standard error are computed pooling all tracks per genotype. This parameter was used to calculate estimated run length.

Estimated Run Length (in μm). Is the average duration-weighted segmental velocity divided by the corrected pause frequency. Since observed run lengths were in many instances invariably truncated due to the limits of a fixed microscope field-of-view, and due to the finite time of image acquisition, to test whether KLC2 shRNA neurons also had decreased run lengths, we calculated estimated run lengths as the average duration-weighted segmental velocity divided by the average corrected pause frequency. These values are more representative of the true run lengths that particles would travel if

we were to image them without sampling constraints. This parameter is a bulk value, so no standard errors can be calculated.

Corrected Pause Frequency (in times/second). Pause frequency is calculated for individual segments as one divided by the moving time of the segment immediately preceding that pause. For each genotype, pause frequency is calculated for each anterograde and retrograde segment pause (including in reversals), and averaged. Standard error is calculated for all segmental pause frequencies per genotype.

Switch Frequency (times/second). The number of reversals a particle undergoes per second. Switch frequency is calculated for each track and averaged per genotype. Standard error is calculated per track.

Motor Colocalization and Vesicle Mapping Data Analyses

Hippocampal cells stained with antibodies against PrP^C, KLC1, and DHC1 were assessed for colocalization. Image pre-processing for 'motor colocalization' and 'vesicle mapping' analyses of stained vesicles was done in ImageJ (NIH). We then fit 2D Gaussian distributions (Thomann et al., 2002) to all point sources from each channel using a custom algorithm (Jaqaman et al., 2008). This resulted in precise estimates of point source positions in each channel. We then designed a method to assess colocalization between PrP^C and KLC1 and/or DHC1 by first taking the Gaussian-fitted coordinates in the PrP^C channel, and determining colocalization with the other channels within a 300 nm radius of each Gaussian-fitted PrP^C puncta (L.S., S.E.E., unpublished data). We defined colocalization within a 300 nm cut-off based on the diffraction-limits of the microscope, and assuming that the size of PrP^C vesicles is below this limit. Cluster mode-fitting of non-normal Gaussian intensity amplitudes was done in MATLAB.

Gaussian Fitting and Cluster Analysis of Segmental Velocity Distributions and Intensity Amplitudes

Intensity amplitudes for all PrP^C vesicles associated with KLC1 and/or DHC1, and segmental velocity distributions of YFP-PrP^C vesicles were non-normal and were fitted with two or three Gaussian modes using the MCLUST package in the R statistical computing environment. Optimal fits were selected using the Bayesian Information Criterion (BIC) analysis, a robust statistic based on model-based clustering, that allows comparison of models with differing clusters (Fraley, 1999). To test the internal consistency of the BIC method, we bootstrapped the original intensity and velocity distributions to create 40 resampled distributions. We obtained the same number of predicted cluster modes for 68-80% of the distributions. Generating a higher number of bootstrapped distributions will likely increase the percent of distributions with the original mode designations.

Gaussian Intensity Amplitude Mode Designation

Intensity amplitudes for all PrP^C vesicles associated with KLC1 and/or DHC1, and segmental velocity distributions were non-normal and were fitted with three Gaussian modes. The assignment of vesicles to each mode was done after calculating threshold values for the intersection between two Gaussian curves (red open circles in Figures 5E, and 5F), using published threshold equations (Moore and McCabe, 2005).

SUPPLEMENTAL REFERENCES

Baas, P.W., Black, M.M., and Banker, G.A. (1989). Changes in microtubule polarity orientation during the development of hippocampal neurons in culture. J. Cell Biol. *109*, 3085-3094.

Baas, P.W., Deitch, J.S., Black, M.M., and Banker, G.A. (1988). Polarity orientation of microtubules in hippocampal neurons: uniformity in the axon and nonuniformity in the dendrite. Proc. Natl. Acad. Sci. U. S. A. *85*, 8335-8339.

Borchelt, D.R., Davis, J., Fischer, M., Lee, M.K., Slunt, H.H., Ratovitsky, T., Regard, J., Copeland, N.G., Jenkins, N.A., Sisodia, S.S*., et al.* (1996). A vector for expressing foreign genes in the brains and hearts of transgenic mice. Genet. Anal. *13*, 159-163.

Cui, J., Wang, Z., Cheng, Q., Lin, R., Xin-Mei, Z., Leung, P.S., Copeland, N.G., Jenkins, N.A., Yao, K.M., and Huang, J.D. (2010). Targeted Inactivation of Kinesin-1 in Pancreatic {beta}-Cells in vivo Leads to Insulin Secretory Deficiency. Diabetes. doi: 10.2337/db09-1078

Falzone, T.L., Stokin, G.B., Lillo, C., Rodrigues, E.M., Westerman, E.L., Williams, D.S., and Goldstein, L.S. (2009). Axonal stress kinase activation and tau misbehavior induced by kinesin-1 transport defects. J. Neurosci. *29*, 5758-5767.

Fraley, C. (1999). MCLUST: Software for Model-Based Cluster Analysis. Journal of Classification *16*, 297-306.

Glater, E.E., Megeath, L.J., Stowers, R.S., and Schwarz, T.L. (2006). Axonal transport of mitochondria requires milton to recruit kinesin heavy chain and is light chain independent. J. Cell Biol. *173*, 545-557.

Jaqaman, K., Loerke, D., Mettlen, M., Kuwata, H., Grinstein, S., Schmid, S.L., and Danuser, G. (2008). Robust single-particle tracking in live-cell time-lapse sequences. Nat. Methods *5*, 695-702.

Klein, R., Smeyne, R.J., Wurst, W., Long, L.K., Auerbach, B.A., Joyner, A.L., and Barbacid, M. (1993). Targeted disruption of the trkB neurotrophin receptor gene results in nervous system lesions and neonatal death. Cell *75*, 113-122.

Moore, D.S., and McCabe, G.P. (2005). Introduction to the Practice of Statistics, 5th edition., 5th edition edn (W. H. Freeman).

Peretz, D., Williamson, R.A., Matsunaga, Y., Serban, H., Pinilla, C., Bastidas, R.B., Rozenshteyn, R., James, T.L., Houghten, R.A., Cohen, F.E*., et al.* (1997). A conformational transition at the N terminus of the prion protein features in formation of the scrapie isoform. J. Mol. Biol. *273*, 614-622.

Rahman, A., Friedman, D.S., and Goldstein, L.S. (1998). Two kinesin light chain genes in mice. Identification and characterization of the encoded proteins. J. Biol. Chem. *273*, 15395-15403.

Rahman, A., Kamal, A., Roberts, E.A., and Goldstein, L.S. (1999). Defective kinesin heavy chain behavior in mouse kinesin light chain mutants. J. Cell Biol. *146*, 1277-1288.

Tanaka, Y., Kanai, Y., Okada, Y., Nonaka, S., Takeda, S., Harada, A., and Hirokawa, N. (1998). Targeted disruption of mouse conventional kinesin heavy chain, kif5B, results in abnormal perinuclear clustering of mitochondria. Cell *93*, 1147-1158.

Taylor, A.M., Blurton-Jones, M., Rhee, S.W., Cribbs, D.H., Cotman, C.W., and Jeon, N.L. (2005). A microfluidic culture platform for CNS axonal injury, regeneration and transport. Nat. Methods *2*, 599-605.

Thomann, D., Rines, D.R., Sorger, P.K., and Danuser, G. (2002). Automatic fluorescent tag detection in 3D with super-resolution: application to the analysis of chromosome movement. J. Microsc. *208*, 49-64.

Xia, C., Rahman, A., Yang, Z., and Goldstein, L.S. (1998). Chromosomal localization reveals three kinesin heavy chain genes in mouse. Genomics *52*, 209-213.

Xia, C.H., Roberts, E.A., Her, L.S., Liu, X., Williams, D.S., Cleveland, D.W., and Goldstein, L.S. (2003). Abnormal neurofilament transport caused by targeted disruption of neuronal kinesin heavy chain KIF5A. J. Cell Biol. *161*, 55-66.

Figure S1.

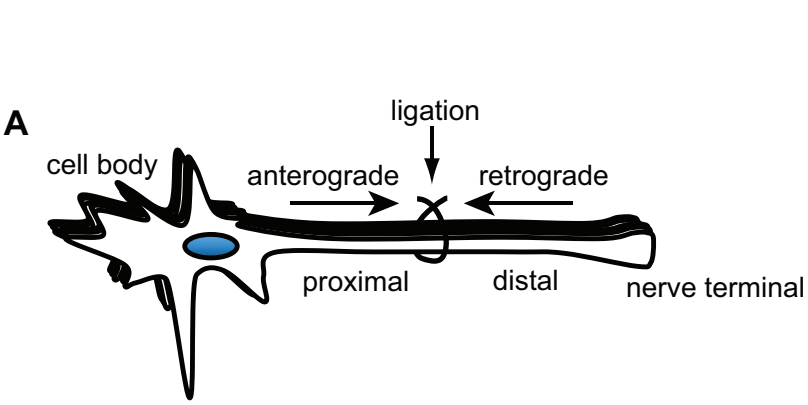
A
ligation
cell body
anterograde
retrograde
proximal
distal
nerve terminal

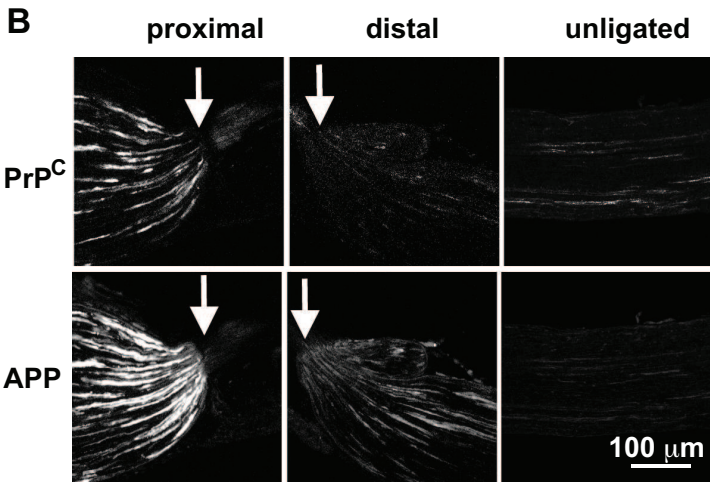
B
proximal
distal
unligated
PrP^C
APP
100 μm

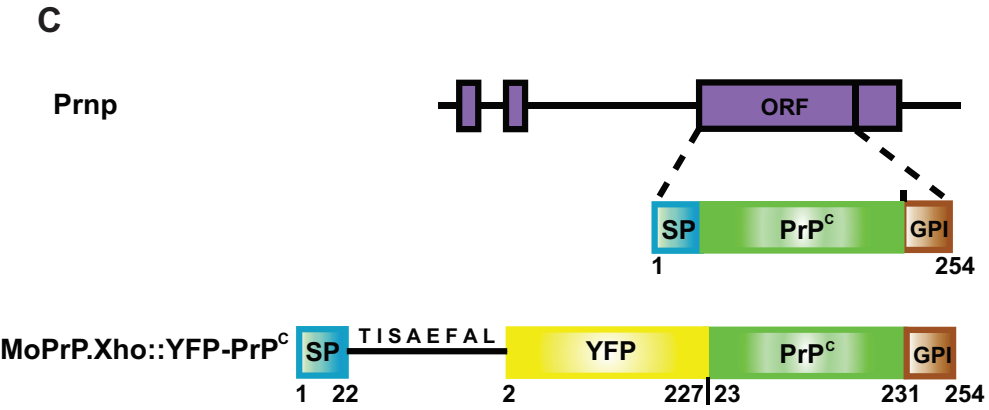
C
Prnp
ORF
SP
PrP^C
GPI
1
254
MoPrP.Xho::YFP-PrP^C
SP
TISAEFAL
YFP
PrP^C
GPI
1 22 2 227 23 231 254

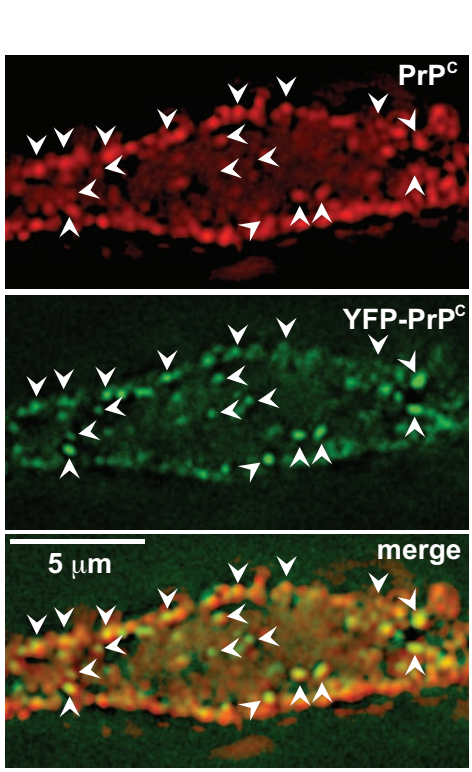
D
PrP^C
YFP-PrP^C
5 μm
merge

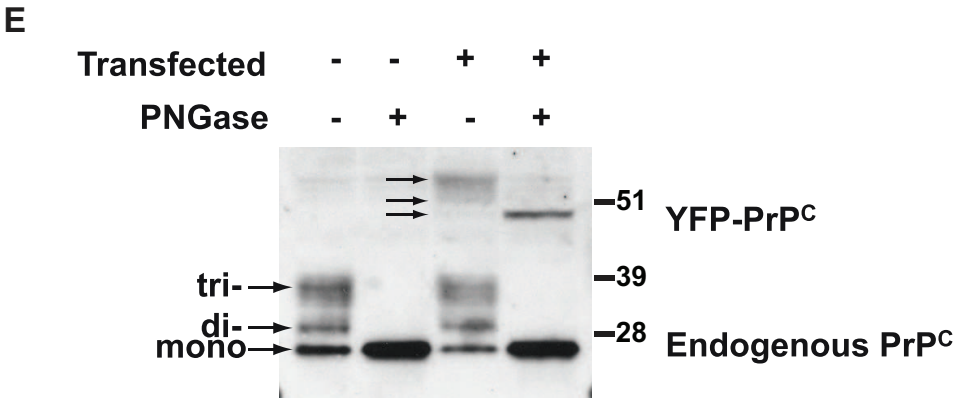
E
Transfected - - + +
PNGase - + - +
tri-
di-
mono
51
39
28
YFP-PrP^C
Endogenous PrP^C

Figure S2.

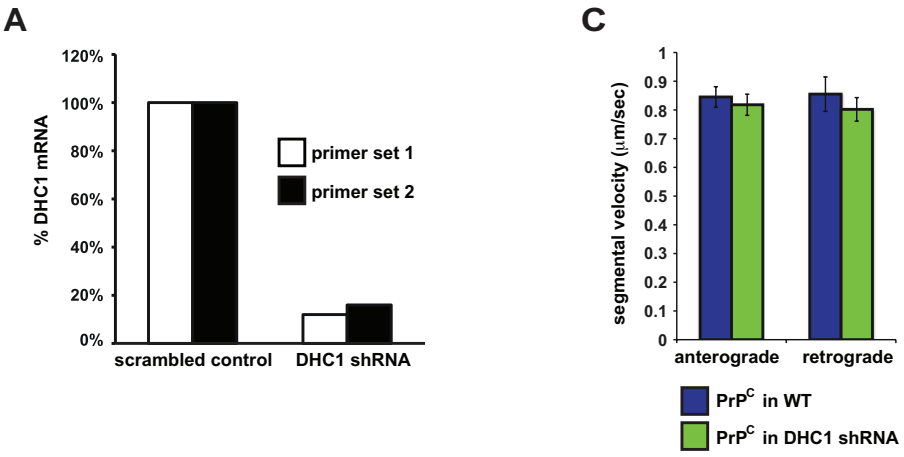
A
120%
100%
80%
60%
40%
20%
0%
% DHC1 mRNA
primer set 1
primer set 2
scrambled control
DHC1 shRNA
C
segmental velocity (μm/sec)
1
0.9
0.8
0.7
0.6
0.5
0.4
0.3
0.2
0.1
0
anterograde
retrograde
PrP^C in WT
PrP^C in DHC1 shRNA

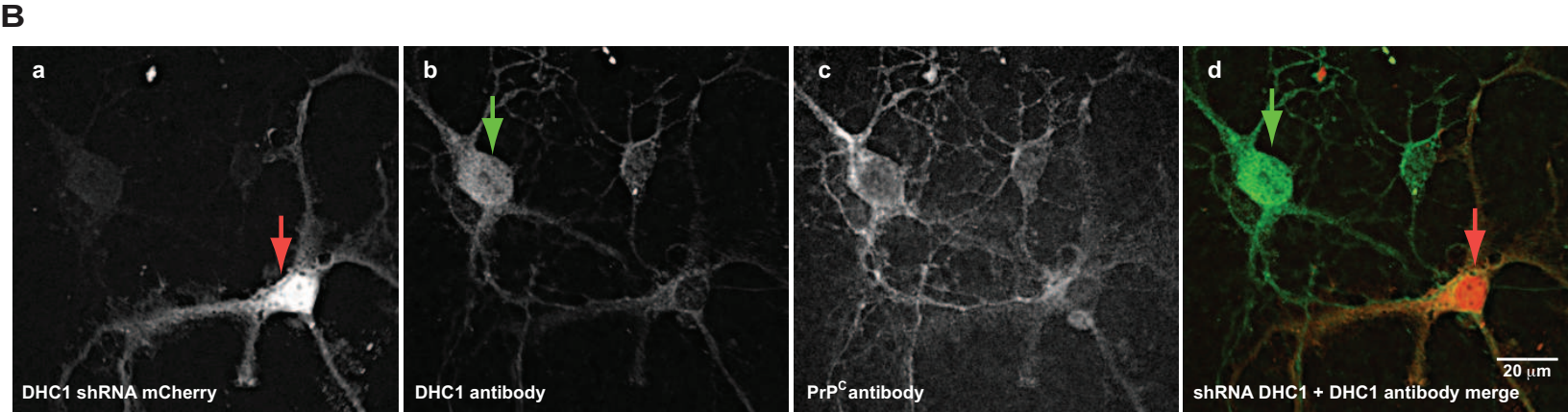
B
a
DHC1 shRNA mCherry
b
DHC1 antibody
c
PrP^C antibody
d
shRNA DHC1 + DHC1 antibody merge
20 μm

Figure S3.

YFP-PrP^C :

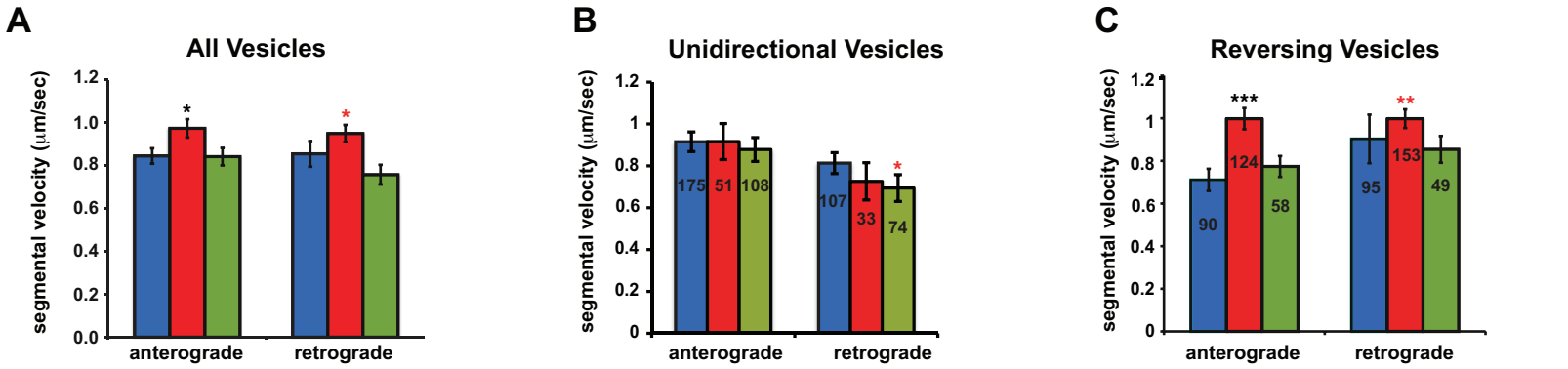

synaptophysin-mCherry:

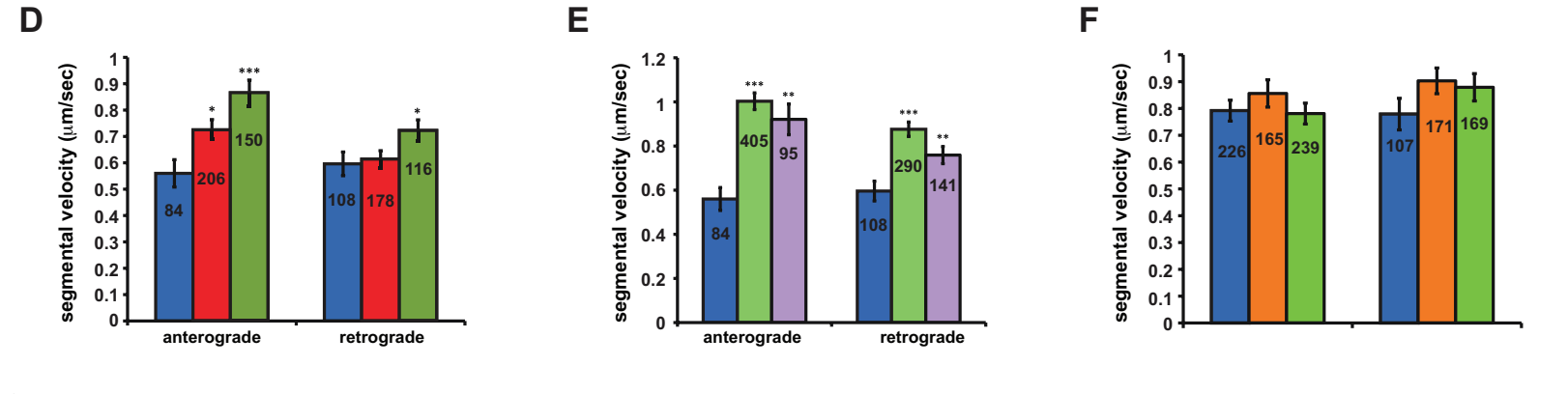

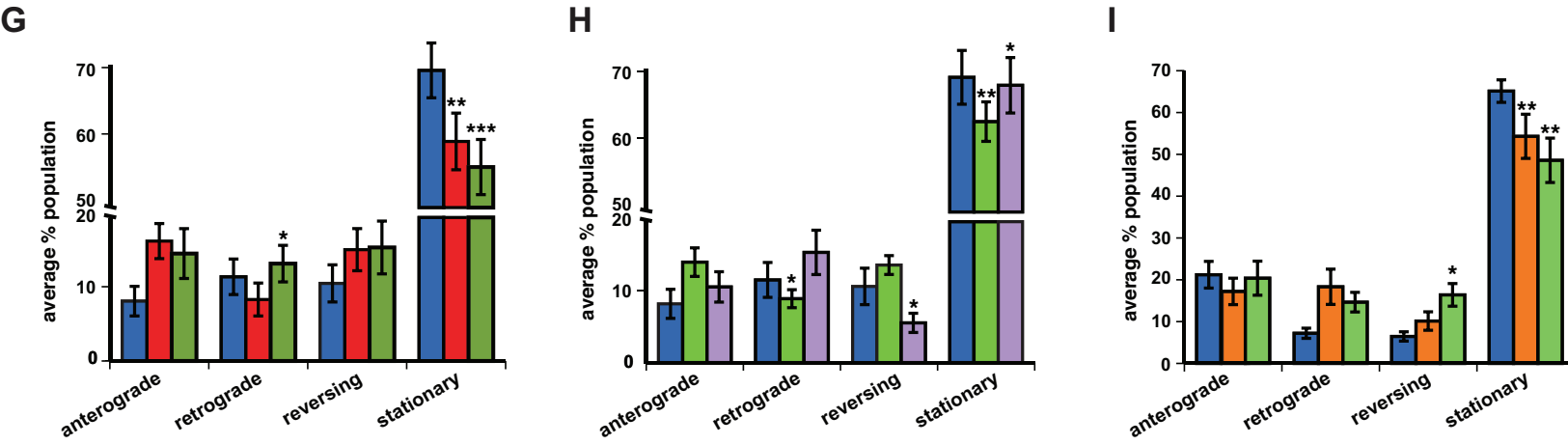

total Nv WT = 293
total Nv KLC1 -/- = 428
total Nv KLC2 shRNA = 211

PrP^C in WT
PrP^C in KLC1 -/-
PrP^C in KLC2 shRNA

total Nv WT = 293
total Nv Kinesin-1A -/- = 894
total Nv Kinesin-1C -/- = 383

PrP^C in WT
PrP^C in Kinesin-1A -/-
PrP^C in Kinesin-1C -/-

total Nv Kinesin-1B-cre 0 MOI = 428
total Nv Kinesin-1B-cre 100 MOI = 309
total Nv Kinesin-1B-cre 400 MOI = 319

PrP^C in Kinesin-1B-cre 0 MOI
PrP^C in Kinesin-1B-cre 100 MOI
PrP^C in Kinesin-1B-cre 400 MOI

Figure S4.

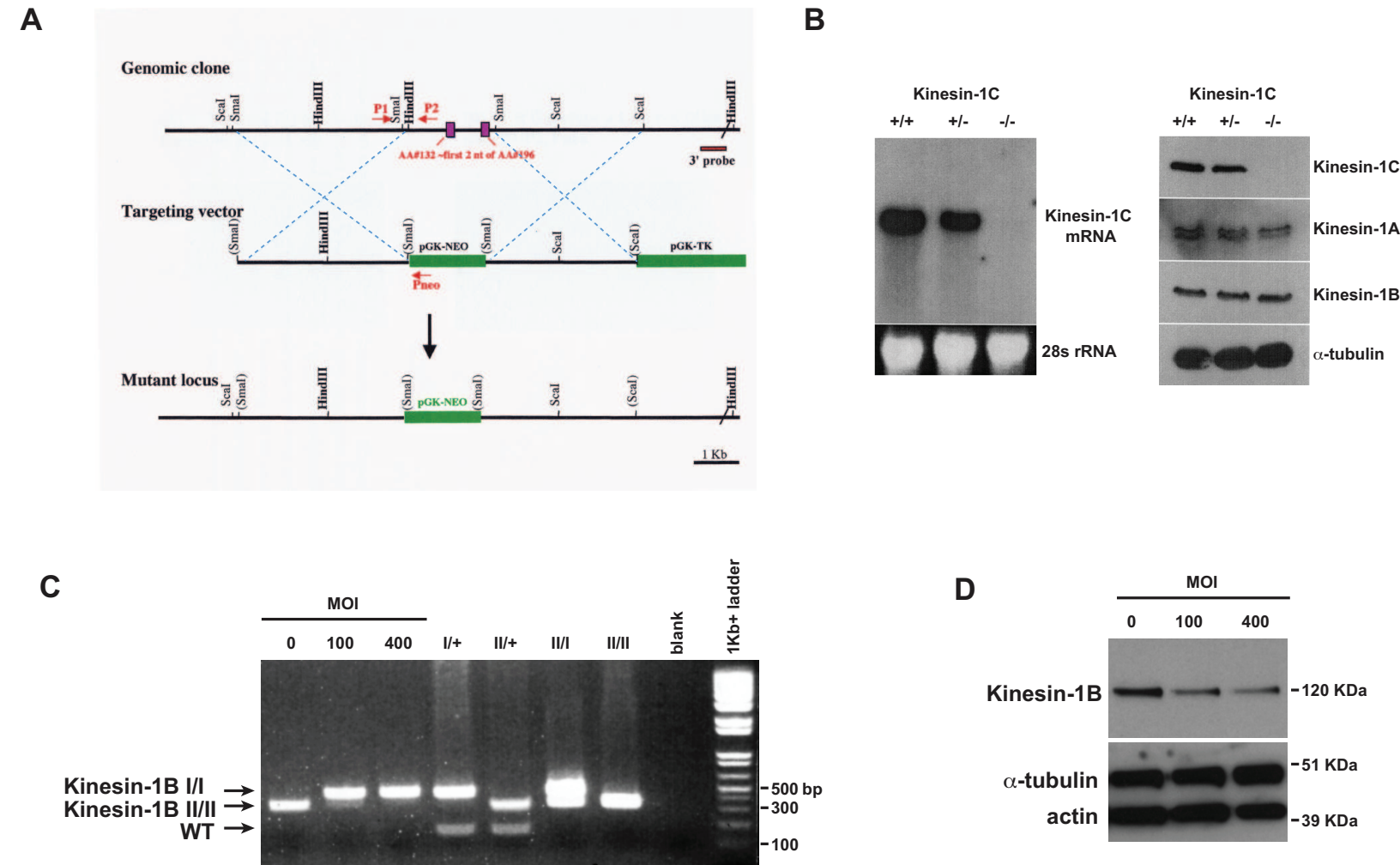
A
Genomic clone
ScaI
SmaI
HindIII
P1
P2
AA#132 -first 2 nt of AA#196
3' probe
Targeting vector
(SmaI)
pGK-NEO
Pneo
pGK-TK
(ScaI)
Mutant locus
1 Kb
B
Kinesin-1C
+/+
+/-
-/-
Kinesin-1C mRNA
28s rRNA
Kinesin-1A
Kinesin-1B
α-tubulin
C
MOI
0
100
400
I/+
II/+
II/I
II/II
blank
1Kb+ ladder
Kinesin-1B I/I
Kinesin-1B II/II
WT
500 bp
300
100
D
MOI
0
100
400
Kinesin-1B
120 KDa
α-tubulin
actin
51 KDa
39 KDa

Figure S5.

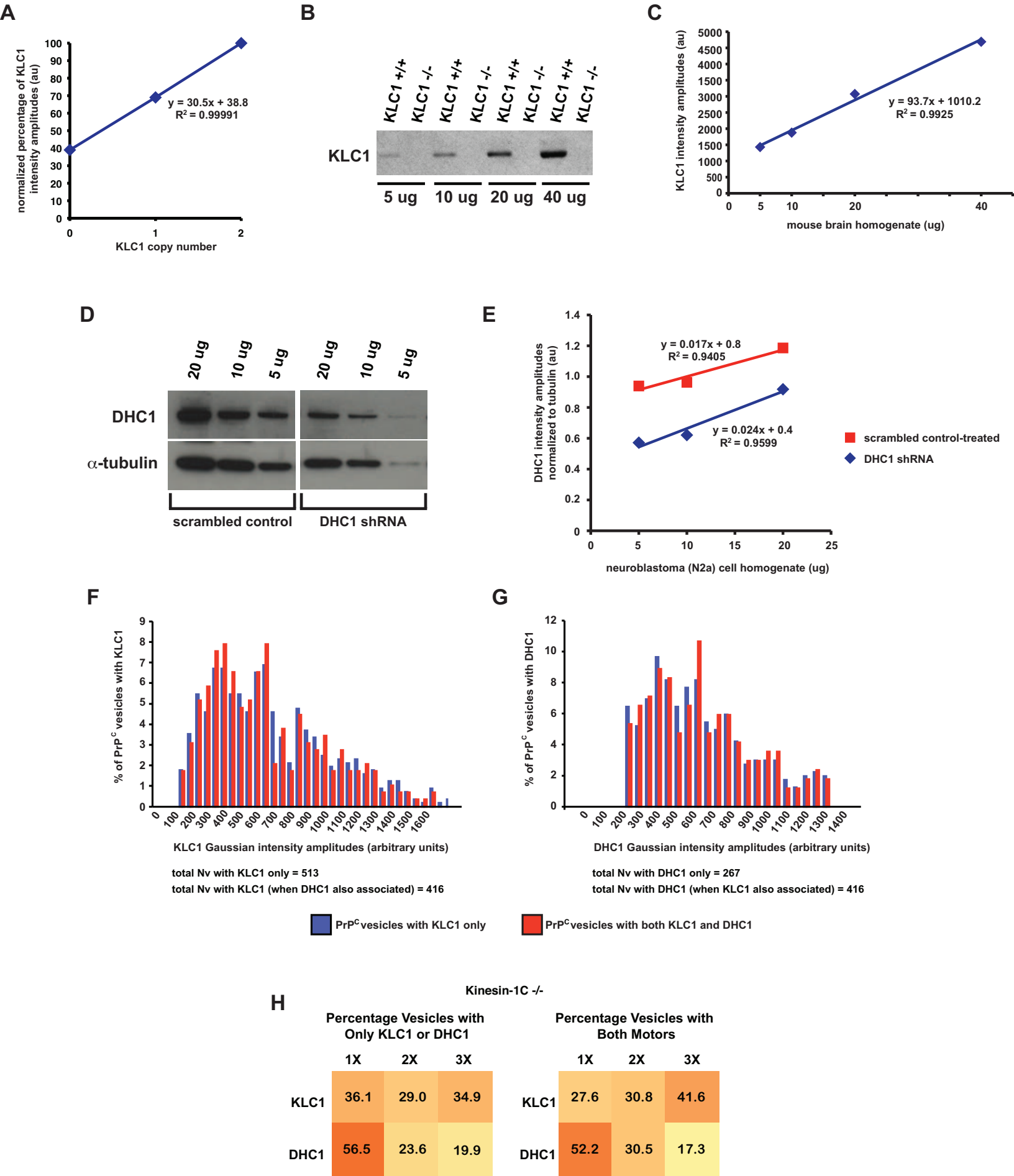
A
normalized percentage of KLC1 intensity amplitudes (au)
y = 30.5x + 38.8
R² = 0.99991
KLC1 copy number
B
KLC1 +/+
KLC1 -/-
KLC1 +/+
KLC1 -/-
KLC1 +/+
KLC1 -/-
KLC1 +/+
KLC1 -/-
KLC1
5 ug
10 ug
20 ug
40 ug
C
KLC1 intensity amplitudes (au)
y = 93.7x + 1010.2
R² = 0.9925
mouse brain homogenate (ug)
D
20 ug
10 ug
5 ug
20 ug
10 ug
5 ug
DHC1
α-tubulin
scrambled control
DHC1 shRNA
E
DHC1 intensity amplitudes normalized to tubulin (au)
y = 0.017x + 0.8
R² = 0.9405
y = 0.024x + 0.4
R² = 0.9599
scrambled control-treated
DHC1 shRNA
neuroblastoma (N2a) cell homogenate (ug)
F
% of PrP^C vesicles with KLC1
KLC1 Gaussian intensity amplitudes (arbitrary units)
total Nv with KLC1 only = 513
total Nv with KLC1 (when DHC1 also associated) = 416
G
% of PrP^C vesicles with DHC1
DHC1 Gaussian intensity amplitudes (arbitrary units)
total Nv with DHC1 only = 267
total Nv with DHC1 (when KLC1 also associated) = 416
PrP^C vesicles with KLC1 only
PrP^C vesicles with both KLC1 and DHC1
H
Kinesin-1C -/-
Percentage Vesicles with Only KLC1 or DHC1
1X 2X 3X
KLC1 36.1 29.0 34.9
DHC1 56.5 23.6 19.9
Percentage Vesicles with Both Motors
1X 2X 3X
KLC1 27.6 30.8 41.6
DHC1 52.2 30.5 17.3